Experimental Investigation of Quantum $\mathcal{PT}$-Enhanced Sensor

Shang Yu,[1,2,3] Yu Meng,[1,2] Jian-Shun Tang,[1,2,*] Xiao-Ye Xu,[1,2] Yi-Tao Wang,[1,2] Peng Yin,[1,2] Zhi-Jin Ke,[1,2] Wei Liu,[1,2] Zhi-Peng Li,[1,2] Yuan-Ze Yang,[1,2] Geng Chen,[1,2] Yong-Jian Han,[1,2] Chuan-Feng Li,[1,2,†] and Guang-Can Guo[1,2]

[1]*CAS Key Laboratory of Quantum Information, University of Science and Technology of China, Hefei, 230026, China*

[2]*CAS Center For Excellence in Quantum Information and Quantum Physics, University of Science and Technology of China, Hefei, 230026, People's Republic of China*

[3]*Research Center for Quantum Sensing, Zhejiang Lab, Hangzhou, 310000, People's Republic of China*

(Received 3 January 2020; accepted 6 November 2020; published 10 December 2020)

$\mathcal{PT}$-symmetric theory is developed to extend quantum mechanics to a complex region, but it wins its great success first in classical systems, for example, optical waveguides and electric circuits, etc., because there are so many counterintuitive phenomena and striking applications, including unidirectional light transport, $\mathcal{PT}$-enhanced sensors (one kind of exceptional-point-based sensor), and wireless power transfer. However, these phenomena and applications are mostly based on the ability to approach a $\mathcal{PT}$-symmetric broken region, which makes it difficult to transfer them to the quantum regime, since the broken quantum $\mathcal{PT}$-symmetric system has not been constructed effectively, until recently several methods have been raised. Here, we construct a quantum $\mathcal{PT}$-symmetric system assisted by weak measurement, which can effectively transit from the unbroken region to the broken region. The full energy spectrum including the real and imaginary parts is directly measured using weak values. Furthermore, based on the ability of approaching a broken region, we for the first time translate the previously mentioned $\mathcal{PT}$-enhanced sensor into the quantum version, and investigate its various features that are associated to the optimal conditions for sensitivity enhancement. In this experiment, we obtain an enhancement of 8.856 times over the conventional Hermitian sensor. Moreover, by separately detecting the real and imaginary parts of energy splitting, we can derive the additional information of the direction of perturbations. Our work paves the way of leading classical interesting $\mathcal{PT}$ phenomena and applications to their quantum counterparts. More generally, since the $\mathcal{PT}$ system is a subset of non-Hermitian systems, our work will be also helpful in the studies of general exception point in the quantum regime.

DOI: 10.1103/PhysRevLett.125.240506

Parity-time ($\mathcal{PT}$)-symmetric theory was developed to extend the quantum mechanics to a complex region [1,2]. In conventional quantum theory, Hermiticity of the Hamiltonian is one of the most basic requirements, which guarantees the physical conditions of real energy and conserved total probability. Alternatively, Hamiltonians satisfying $\mathcal{PT}$ symmetry (generally non-Hermitian) also fulfill these two conditions with the inner product of states redefined. This is the so-called $\mathcal{PT}$-symmetric theory. For some special situations, this theory can collapse to the conventional quantum theory.

Although designed for the purpose of improving quantum theory, $\mathcal{PT}$-symmetric theory wins its great success in classical systems including electronic circuits [3], and especially optical systems such as the optical waveguide [4,5], microcavity [6,7], and laser systems [8–10], etc., due to the similarity between their master equations and the $\mathcal{PT}$-symmetric Schrödinger equation. The balanced gain-and-loss mechanism plays a critical role in these systems. Not only aiming to the goal of studying $\mathcal{PT}$-symmetric theory, these systems attracted a lot of interest also because they exhibit many striking and counterintuitive phenomena and indicate a lot of new applications, for example, the unidirectional invisibility [11–13] and nonreciprocal light propagation [6,7], the $\mathcal{PT}$-symmetric single-mode lasers [9,10] and laser absorber [8,14], and the wireless power transfer [15], etc. Actually, we want to note that the $\mathcal{PT}$-symmetric system is only a subset of the larger class of non-Hermitian systems [16–27], and many unique features and applications of the $\mathcal{PT}$-symmetric system are inherited from its non-Hermitian property, but not restricted to the $\mathcal{PT}$-symmetric system, for example, the exceptional-point (EP)-enhanced sensor [19–21] and its variant applications in microscopic-thermal-mapping systems [22], wireless-sensing systems [23–25], and the optical gyroscope [26,27], etc. The $\mathcal{PT}$-symmetric system plays as an excellent platform for the studies of EP, including the EP-enhanced sensor, which in this case we simply call the $\mathcal{PT}$-enhanced sensor [20].

However, these fantastic phenomena and applications cannot be directly introduced into quantum regime where the $\mathcal{PT}$-symmetric theory was born. This is primarily due to that the gain-and-loss configuration is difficult to transfer to the quantum regime directly since the single photon

 © 2020 American Physical Society

cannot be copied (i.e., no gain here), and most of the classical $\mathcal{PT}$ applications mentioned above emerge usually in the $\mathcal{PT}$-symmetry-broken region which just relies on gain and loss.

In the quantum regime, there are its own simulation methods and striking predictions, but most of these predicted proposals are in the unbroken region, for example, the ultrafast transformation between two orthogonal states [28], the quantum discrimination with single-shot measurement [29] and the potential violation of the no-signaling principle [30,31]. The first experimental simulation of $\mathcal{PT}$-symmetric evolution in the quantum regime is realized by Tang *et al.* in 2016 [31]. Although by using this method and the later similar variants [32] the broken region can be reached, these methods are more like the maps that only consider the initial and final states, but not the whole evolution. On the other hand, the Naimark-dilation method is proposed and developed [33,34]. Its main idea is to embed the $\mathcal{PT}$-symmetric system into a larger Hermitian system, and the whole evolution of the Hermitian system represents the sub-$\mathcal{PT}$-symmetric system's evolution, then the evolved results can be read out by postselection. The drawback of this method is that it still cannot reach the broken region, therefore, the purpose to transfer the splendid phenomena and applications of the classical regime to the quantum regime is still unachievable.

Until recently, several methods appear to extend the quantum $\mathcal{PT}$-symmetric system to the broken region also by embedding the $\mathcal{PT}$ one into a larger Hermitian system [35,36]. Among these methods, one theoretical proposal [36] suggests that the weak measurement is used to read out the information of the embedded $\mathcal{PT}$-symmetric system. As is well known, weak measurement is another powerful tool to show many striking phenomena and applications, e.g., directly measuring of the wave function of a photon [37] or entangled photon pair [38], directly measuring the density matrix [39], etc.

In this work, we use the weak values to directly characterize the energy spectrum of the quantum $\mathcal{PT}$-symmetric system through unbroken to broken regions in experiment. On the basis of this ability to approach the broken region, we for the first time transfer the $\mathcal{PT}$-enhanced sensor in the classical regime to the quantum regime. The classical version of the proposal [19] and the later experiments [20,21] are based on the microcavities in the gain-and-loss scheme (note that Refs. [19,21] are not restricted to a $\mathcal{PT}$-symmetrical system, and Ref. [20] is performed in a $\mathcal{PT}$-symmetrical system), but the EP and diabolic point (DP) are the common conceptions in both regimes, which will be further explained later. In our experiment, we investigate in detail the various influences of the parameters in the Hamiltonian and perturbation to the enhancement of sensitivity, and obtain a maximal enhancement of 8.856 times based on our experimental conditions.

First of all, we would like to briefly recall some related conceptions of the $\mathcal{PT}$-enhanced sensor. The conventional sensor is based on DP, which means a twofold degenerate point for the eigenenergies of a Hermitian system, and a small perturbation ϵ will lift this degeneracy and cause an energy splitting proportional to ϵ [19]. This splitting then can be used to sense the small perturbation. Obviously, the eigenstates here are orthogonal. In contrast, for a non-Hermitian system, there exists another degenerate point called EP, which can also be used to construct a sensor for perturbation ϵ (i.e., an EP-enhanced sensor, or $\mathcal{PT}$-enhanced sensor if it is a $\mathcal{PT}$-symmetric system). The difference is that, at this point, not only the eigenenergies but also the eigenstates coalesce. Moreover, the (second-order) EP-induced energy splitting is proportional to the square root of $|\epsilon|$, whereas the DP-induced splitting is proportional to $|\epsilon|$. This makes the EP sensor more sensitive. Considering a $\mathcal{PT}$-symmetric system, as the perturbations could direct this system to either unbroken or broken regions, the realization of a $\mathcal{PT}$-symmetry-breaking case should therefore be very necessary now.

Next, we will discuss the method to construct a $\mathcal{PT}$-symmetric system with both unbroken and broken regions using weak measurement. Given a $\mathcal{PT}$-symmetric Hamiltonian $H_{\mathcal{PT}}$ (denoted as H for short below) and a state $|\varphi\rangle$, the purpose of this section is to directly measure the expectation value of H on $|\varphi\rangle$, i.e., $\langle\varphi|H|\varphi\rangle_\eta$, where $\langle\varphi_1|H|\varphi_2\rangle_\eta \equiv \langle\varphi_1|\eta H|\varphi_2\rangle$ represents the η-inner product [2,36]. Without loss of generality, a two-level $\mathcal{PT}$-symmetric Hamiltonian can be chosen as

$$H = \begin{pmatrix} re^{i\theta} & s \\ s & re^{-i\theta} \end{pmatrix}, \tag{1}$$

where s, r (we set $r > 0$ here), θ are real [40]. The eigenenergies are $E_\pm = r\cos\theta \pm \sqrt{s^2 - r^2\sin^2\theta}$, and when $|s| \geq |r\sin\theta|$, the symmetry is unbroken, otherwise, it is broken. The point $|s| = |r\sin\theta|$ is proven to be an EP as mentioned above.

The two primary bases of this method are (i) the equivalence of the expectation value of H on $|\varphi\rangle$ and the weak value of a specially dilated Hamiltonian $\tilde{H}$ on the preselected state $|\tilde{\varphi}_i\rangle = \binom{|\varphi\rangle}{|\varphi\rangle}$ and postselected state $|\tilde{\varphi}_f\rangle = \binom{|\varphi'\rangle}{|\varphi''\rangle}$ that are also specially dilated from $|\varphi\rangle$, i.e., $\langle\varphi|H|\varphi\rangle_\eta = \langle\tilde{\varphi}_f|\tilde{H}|\tilde{\varphi}_i\rangle / \langle\tilde{\varphi}_f|\tilde{\varphi}_i\rangle \equiv \langle\tilde{H}\rangle_{\mathrm{w}}$ [36,41]; (ii) the derivation of the weak value of the dilated Hamiltonian $\tilde{H}$ through weakly coupling and detecting a pointer ancilla (here a qubit). The interaction Hamiltonian of the coupled systems of the pointer $\hat{P}$ and the dilated system $\tilde{H}$ can be written as $H_{\mathrm{int}} = \tilde{H} \otimes \hat{P}$. It is proved that, after the preselection, weak coupling, and postselection, the real and imaginary parts of the desired weak value can be approximately determined by detecting the expectation

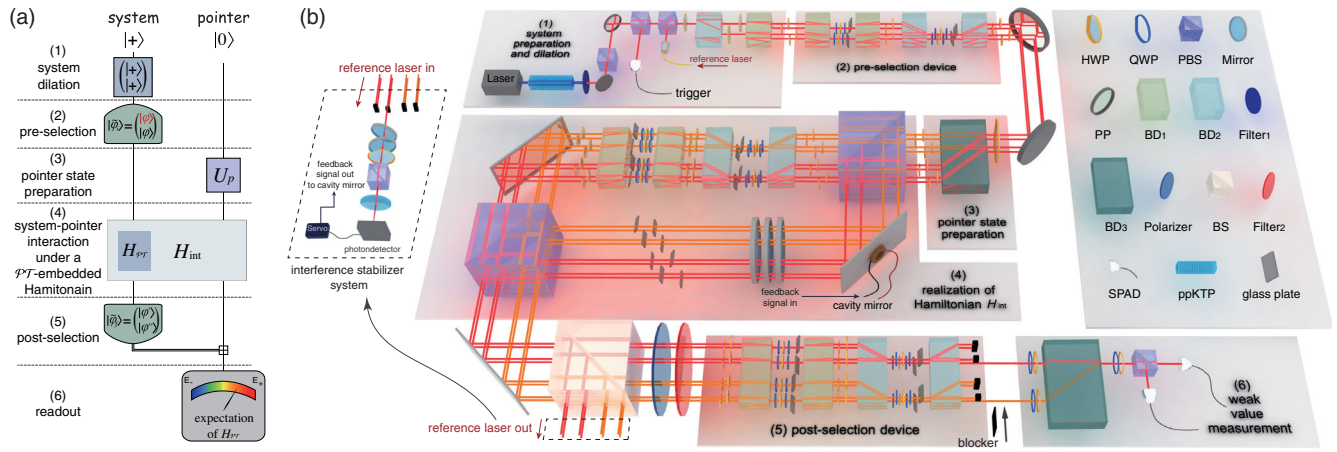

FIG. 1. (a) Logic diagram of the construction of $\mathcal{PT}$-symmetric system. (b) Experimental setup. Both the diagram and setup are divided into 6 modules: (1) The system preparation and dilation; (2) preselection state preparation; (3) pointer state preparation; (4) coupling of the pointer and dilated system in which the $\mathcal{PT}$-symmetric system is embedded; (5) postselection; (6) weak value readout. Half-wave plate (HWP); quarter-wave plate (QWP); beam splitter (BS); polarizing beam splitter (PBS); phase plate (PP); beam displacer (BD); periodically poled potassium titanyl phosphate (ppKTP); band-pass filter (BF); single-photon avalanche diode (SPAD).

values of Pauli observables σ_y and σ_z on the coupled and postselected pointer state, respectively. Details can be found in the Supplemental Material [41].

Knowing these two basic steps, we can construct our $\mathcal{PT}$-symmetric system as that shown in Fig. 1. As labeled in the figures, there are 6 modules. (1) The photon is generated by spontaneous parametric down conversion (SPDC), and the path state is dilated from two-dimensional space to four-dimensional space. (2) The preselection state $|\tilde{\varphi}_i\rangle = (\begin{smallmatrix}|\varphi\rangle\\|\varphi_i\rangle\end{smallmatrix})$ is prepared using a four-port interferometer (note: this interferometer can realize arbitrary unitary evolution [41]). (3) The pointer state $|P_i\rangle$ is prepared using a large-size BD. (4) The weak coupling evolution $e^{-igH_{\rm int}} \approx I - ig\hat{H} \otimes \hat{P}$ is performed in a big locked interferometer containing two small four-port interferometers [50]. (5) The state after evolution $(I - ig\tilde{H} \otimes \hat{P})|\tilde{\varphi}_i\rangle|P_i\rangle$ is projected into the postselection state $|\tilde{\varphi}_f\rangle = (\begin{smallmatrix}|\varphi'\rangle\\|\varphi''\rangle\end{smallmatrix})$, realized using two four-port interferometers, and the final pointer state $|P_f\rangle$ is derived. (6) The real and imaginary parts of weak value $\langle\tilde{H}\rangle_{\rm w}$ (i.e., $\langle\varphi|H|\varphi\rangle_\eta$) is read out directly by measuring the expectations of σ_y and σ_z on $|P_f\rangle$, respectively. Details are found in the Supplemental Material, Sec. I [41].

With this method and experimental setup at hand, we can now first directly depict the energy spectrum $E_\pm(s)$ of the $\mathcal{PT}$-symmetric system governed by $H(s)$ [Eq. (1)] with r, θ being the fixed parameters and s being the variable. It is easy to prove that the real and imaginary parts of E_+ provide the upper bounds for the corresponding parts of the expectation value $\langle\varphi|H|\varphi\rangle_\eta$, respectively, when $|\varphi\rangle$ is varied; and the real and imaginary parts of E_- provide the lower bounds. Therefore, we just need to find the expectation values with maximal or minimal real and imaginary parts, denoted as $\langle\varphi|H|\varphi\rangle_\eta^+ = \langle\tilde{H}\rangle_{\rm w}^+ = E_+$ and $\langle\varphi|H|\varphi\rangle_\eta^- = \langle\tilde{H}\rangle_{\rm w}^- = E_-$ (see Supplemental Material for details [41]). In this section, we set $r = \sqrt{2}$ and $\theta = \pi/4$, and the real and imaginary parts of $\langle\tilde{H}\rangle_{\rm w}^+$ (the weak value with maximal real and imaginary parts that are really detected in experiment) are shown in Figs. 2(a) and 2(b), respectively. The black circles with error bars are experimental results of $\langle\tilde{H}\rangle_{\rm w}^+$ (corresponding to the axis and black labels on the left), and the errors are obtained using the Monte Carlo method considering the counting noise and inaccurate wave-plate angle settings (the detailed calculation procedure can be found in Sec. VIII of the Supplemental Material [41]). The red lines are theoretical values of E_+ (corresponding to the axis and red labels on right) calculated from the $\mathcal{PT}$-symmetric Hamiltonian H [Eq. (1)]. The situation of E_- is similar and not shown here.

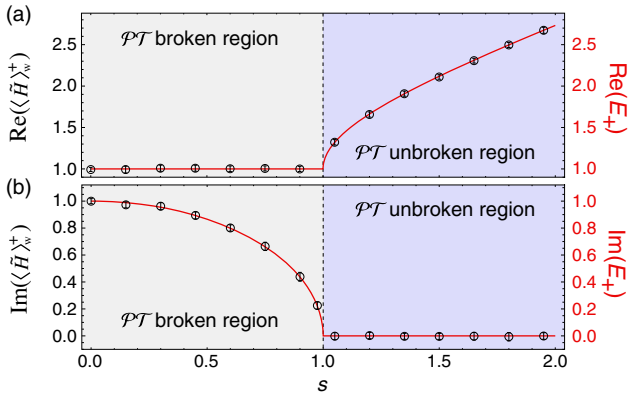

FIG. 2. Energy spectrum $E_+(s)$ of the $\mathcal{PT}$-symmetric system directly measured by weak value $\langle\tilde{H}(s)\rangle_{\rm w}^+$. The black circles with error bars are real and imaginary parts of the weak value, and the red lines are the corresponding eigenenergy directly calculated from the $\mathcal{PT}$-symmetric Hamiltonian Eq. (1); i.e., $E_+(s)|_{r=\sqrt{2},\theta=\pi/4} = 1 + \sqrt{s^2 - 1}$.

When s varies from 2 to 0, we see a continuous transition from the unbroken region to the broken region, and the EP appears at $s = 1$. Namely, when $s > 1$, the imaginary part of the energy always vanishes, and only an s-dependent real part is left (corresponding to the unbroken region); when $s < 1$, in contrast, the imaginary part is nonzero and s dependent, but the real part keeps as a constant (corresponding to broken region).

On the basis of the ability to approach the broken region, as discussed previously, this method can be used to translate some fantastic $\mathcal{PT}$-symmetric phenomena and applications in classical system into quantum regime. One of these phenomena is the $\mathcal{PT}$-enhanced sensor, which was originally proposed [19] and later realized [20] in an optical microcavity system armed with gain-and-loss configuration. Here we translate it into the quantum regime, namely, a quantum $\mathcal{PT}$-enhanced sensor; and study the detailed features of this kind of sensor on our experimental setup, which provides good guidance for the concrete applications on other systems [35], for example, the single defect in crystal or powder which is small enough to sense local tiny perturbations of magnetic or electric fields [51].

To study the quantum $\mathcal{PT}$-enhanced sensor, we need to determine the DP and EP first as that in the classical regime. According to the $\mathcal{PT}$-symmetric Hamiltonian H in Eq. (1), when $\theta = 0$ (here we choose $0 \leq \theta < \pi$), H collapses to a Hermitian Hamiltonian. By calculating the eigensystem of this Hamiltonian, one can find that the two eigenenergies have a cross when s varies, and the cross point is $s = 0$; the eigenstates are always orthogonal. Therefore, this cross point with degenerate energies is just the DP. When $\theta \neq 0$, it is easy to find that at the point $s = r \sin\theta$, i.e., the transition point from unbroken to broken regions, both the eigenenergies and eigenstates coalesce. That is also why we call it EP. Now, we introduce a tiny perturbation Hamiltonian $\epsilon\sigma_x$ (σ_x is Pauli operator) [40] to H at DP or EP. We will see an energy splitting that is proportional to ϵ in the DP case, but not in the EP case. In the EP case, the splitting is more drastic around the point. These energy splittings can be regarded as the appearance of the small perturbation ϵ.

In this section, our purpose is to study the enhancement of sensitivity by using EP compared to the conventionally used DP in the quantum regime. The splittings induced by ϵ perturbation are denoted as ΔE_{EP} and ΔE_{DP} for EP and DP situations, respectively. Similar as that in Ref. [19], we use $|\Delta E_{\mathrm{DP}}|$ with same ϵ to normalize both the real and imaginary parts of ΔE_{EP}. We note that ΔE_{DP} is real since it happens in the Hermitian system. The normalized EP splitting is denoted as $\Delta E(\epsilon) = \Delta E_{\mathrm{EP}}(\epsilon)/|\Delta E_{\mathrm{DP}}(\epsilon)|$ [40]. Obviously, $|\Delta E|$ can be directly regarded as the enhancement coefficient of EP- to DP-related sensitivities.

As discussed above, in the zone of $0 \leq \theta < \pi$, DP is unique, i.e., $\theta = 0$, but EP can vary as θ changes. How do the different EPs affect the enhancement of sensitivity?

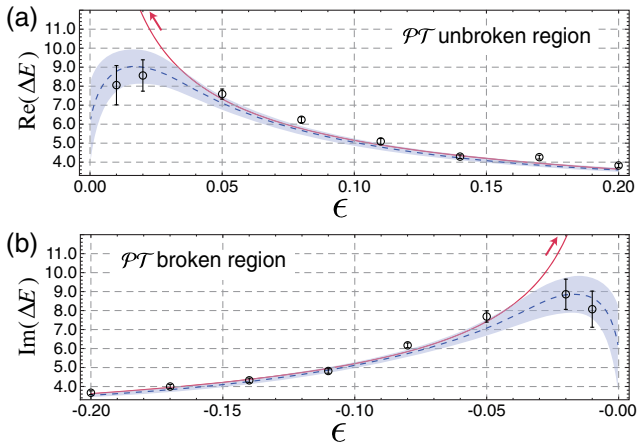

FIG. 3. Response of normalized energy splitting ΔE to amplitude of perturbation ϵ. $r = \sqrt{2}$ and $\theta = \pi/2$. Similarly, only one part does not vanish, and black circles and red lines represent the experimental results and theoretical values, respectively.

By varying θ and detecting the normalized splitting ΔE, we find that when $\theta = \pi/2$ the enhancement will get a maximum; details are introduced in Sec. IX of the Supplemental Material [41]. Therefore, in the following we will fix $\theta = \pi/2$, and specially investigate the response ability of the quantum $\mathcal{PT}$-enhanced sensor over the Hermitian sensor when the perturbation amplitude ϵ is varying, especially the case of tiny ϵ, which attracts quite a lot of interest. The results are shown in Fig. 3, where only the nonvanished parts of ΔE in the unbroken [$\epsilon > 0$, Fig. 3(a)] or broken [$\epsilon < 0$, Fig. 3(b)] regions are presented [52]. The black circles are experimental results, and the red lines are theoretical predictions. Particularly, the blue dashed lines and corresponding light-blue shadows are the numerical-simulation results considering the effect of counting noise and inaccuracy of wave-plate angle settings, with the dashed lines representing the expectation values of 50 simulated enhancement results and the shadows representing the standard deviations. Details can be found in the Supplemental Material [41]. For relatively large ϵ, typically $|\epsilon| > 0.05$, the enhancement of sensitivity (i.e., $|\Delta E|$) increases monotonically as $|\epsilon|$ decreases. For small ϵ, ideally, this enhancement can reach infinity when the perturbation ϵ becomes very tiny, as shown by the red theoretical lines in Fig. 3, since the second-order-EP-induced energy splitting is proportional to the square root of $|\epsilon|$, while the DP-induced splitting is proportional to $|\epsilon|$, however, this is obviously counterintuitive. The experimental results for $|\epsilon| < 0.05$ in Fig. 3 have indicated this point, where we get a maximum of ΔE of 8.594 ± 0.803 for real part and 8.856 ± 0.791 for imaginary part, but not infinity. The answer is the noises. When ϵ is small enough compared to the noise strength, the values of ΔE_{EP} and ΔE_{DP} are never dominated by $\sqrt{|\epsilon|}$ or $|\epsilon|$ any longer, but the noise-induced errors. Even if ϵ goes to zero, the noise will not, therefore, the arbitrary increasing of the

enhancement with arbitrarily small ϵ will be terminated by the noises. Similar discussions are also debated in the classical regime [45–48], with which our conclusion for quantum $\mathcal{PT}$ sensor is coincident. In the Supplemental Material [41], we adopt the numerical-simulation method to study this subject in detail, including the effect of counting noise and inaccurate angle settings (results also shown in Fig. 3 with blue dashed lines and light-blue shadows). The maximal real part of enhancement in the simulation result is 9.055 ± 0.845 at $\epsilon = 0.0171$, which approximately coincides with the previously mentioned experimental result within errors.

In summary, we have experimentally constructed a weak-measurement-assisted $\mathcal{PT}$-symmetric system in the quantum regime, and using weak values the energy spectrum of this system is directly measured, from which we can observe the transition from the unbroken region to the broken region. Using this ability of approaching the broken region, we for the first time translate the striking phenomena and applications of a classical $\mathcal{PT}$-symmetric system into the quantum regime. Concretely, we experimentally investigate a quantum version of the $\mathcal{PT}$-enhanced sensor, whose classical counterpart was proposed and later realized in a coupled microcavity system with gain and loss. In our experiment, the sensitivity is enhanced 8.856 times compared to the conventional Hermitian sensor. Besides the single photons, other quantum systems, including spins in the defects of crystals or nanopowders, can also be used to construct quantum $\mathcal{PT}$ systems [35,49], and hence the quantum EP sensor. These sensors, especially single spin, usually have small sizes compared to classical EP-based sensors, therefore, they can be used to detect the local physical quantities at the single- or few-atom level, such as the magnetic field of single molecule [51]. Our work will provide guidance for the design of this type of high-sensitivity quantum sensors. Moreover, based on the quantum nature of our experiment, entanglement and other quantum resources can be introduced into the $\mathcal{PT}$-enhanced sensor, which will help to further improve the capabilities of this sensor, especially, sensitivity (see the Supplemental Material for details [41]). Our platform can also be used to investigate the quantum versions of other classical $\mathcal{PT}$ phenomena.

We thank Xing Rong, Qiang Li, Zhih-Ahn Jia, and Minyi Huang for insightful discussions. This work is supported by the National Key Research and Development Program of China (Grant No. 2017YFA0304100), the National Natural Science Foundation of China (Grants No. 61327901, No. 11674304, No. 11822408, No. 61490711, No. 11774335, and No. 11821404), the Key Research Program of Frontier Sciences of the Chinese Academy of Sciences (Grant No. QYZDY-SSW-SLH003), the Youth Innovation Promotion Association of Chinese Academy of Sciences (Grant No. 2017492), the Foundation for Scientific Instrument and Equipment Development of Chinese Academy of Sciences (Grant No. YJKYYQ20170032), the Fok Ying Tung Education Foundation (Grant No. 171007), the Science Foundation of the CAS (Grant No. ZDRW-XH-2019-1), the Anhui Initiative in Quantum Information Technologies (Grants No. AHY020100 and No. AHY060300), the National Postdoctoral Program for Innovative Talents (Grant No. BX20180293), China Postdoctoral Science Foundation funded projects (Grants No. 2020M681949, No. 2018M640587), and the Fundamental Research Funds for the Central Universities (Grants No. WK2470000026 and No. WK2470000028).

S. Y. and Y. M. contributed equally to this work.

*tjs@ustc.edu.cn
†cfli@ustc.edu.cn

[1] C. M. Bender and S. Boettcher, Real Spectra in Non-Hermitian Hamiltonians Having $\mathcal{PT}$ Symmetry, Phys. Rev. Lett. **80**, 5243 (1998).
[2] C. M. Bender, D. C. Brody, and H. F. Jones, Complex Extension of Quantum Mechanics, Phys. Rev. Lett. **89**, 270401 (2002).
[3] N. Bender, S. Factor, J. D. Bodyfelt, H. Ramezani, D. N. Christodoulides, F. M. Ellis, and T. Kottos, Observation of Asymmetric Transport in Structures with Active Nonlinearities, Phys. Rev. Lett. **110**, 234101 (2013).
[4] A. Guo, G. J. Salamo, D. Duchesne, R. Morandotti, M. Volatier-Ravat, V. Aimez, G. A. Siviloglou, and D. N. Christodoulides, Observation of $\mathcal{PT}$-Symmetry Breaking in Complex Optical Potentials, Phys. Rev. Lett. **103**, 093902 (2009).
[5] C. E. Rüter, K. G. Makris, R. El-Ganainy, D. N. Christodoulides, M. Segev, and D. Kip, Observation of parity-time symmetry in optics, Nat. Phys. **6**, 192 (2010).
[6] B. Peng, Ş. K. Özdemir, F. Lei, F. Monifi, M. Gianfreda, G. L. Long, S. Fan, F. Nori, C. M. Bender, and L. Yang, Parity-time-symmetric whispering-gallery microcavities, Nat. Phys. **10**, 394 (2014).
[7] L. Chang, X. Jiang, S. Hua, C. Yang, J. Wen, L. Jiang, G. Li, G. Wang, and M. Xiao, Parity-time symmetry and variable optical isolation in active-passive-coupled microresonators, Nat. Photonics **8**, 524 (2014).
[8] Y. D. Chong, Li Ge, and A. D. Stone, $\mathcal{PT}$-Symmetry Breaking and Laser-Absorber Modes in Optical Scattering Systems, Phys. Rev. Lett. **106**, 093902 (2011).
[9] L. Feng, Z. J. Wong, R. Ma, Y. Wang, and X. Zhang, Single-mode laser by parity-time symmetry breaking, Science **346**, 972 (2014).
[10] H. Hodaei, M. Mira, M. Heinrich, D. N. Christodoulides, and M. Khajavikhan, Parity-time-symmetric microring lasers, Science **346**, 975 (2014).
[11] Z. Lin, H. Ramezani, T. Eichelkraut, T. Kottos, H. Cao, and D. N. Christodoulides, Unidirectional Invisibility Induced by $\mathcal{PT}$-Symmetric Periodic Structures, Phys. Rev. Lett. **106**, 213901 (2011).

[12] A. Regensburger, C. Bersch, M.-A. Miri, G. Onishchukov, D. N. Christodoulides, and U. Peschel, Parity-time synthetic photonic lattics, Nature (London) **488**, 167 (2012).
[13] L. Feng, Y.-L. Xu, W. S. Fegadolli, M.-H. Lu, J. E. B. Oliveira, V. R. Almeida, Y.-F. Chen, and A. Scherer, Experimental demonstration of a unidirectional reflectionless parity-time metamaterial at optical frequencies, Nat. Mater. **12**, 108 (2013).
[14] Y. Sun, W. Tan, H. Li, J. Li, and H. Chen, Experimental Demonstration of a Coherent Perfect Absorber with $\mathcal{PT}$ Phase Transition, Phys. Rev. Lett. **112**, 143903 (2014).
[15] S. Assawaaorrait, X. Yu, and S. Fan, Robust wireless power transfer using a nonlinear parity-time-symmetric circuit, Nature (London) **546**, 387 (2017).
[16] J. Doppler, A. A. Mailybaev, J. Böhm, U. Kuhl, A. Girschik, F. Libisch, T. J. Milburn, P. Rabl, N. Moiseyev, and S. Rotter, Dynamically encircling an exceptional point for asymmetric mode switching, Nature (London) **537**, 76 (2016).
[17] M. Brandstetter, M. Liertzer, C. Deutsch, P. Klang, J. Schöberl, H. E. Türeci, G. Strasser, K. Unterrainer, and S. Rotter, Reversing the pump dependence of a laser at an exceptional point, Nat. Commun. **5**, 4034 (2014).
[18] M. Liertzer, L. Ge, A. Cerjan, A. D. Stone, H. E. Tureci, and S. Rotter, Pump-Induced Exceptional Points in Lasers, Phys. Rev. Lett. **108**, 173901 (2012).
[19] J. Wiersig, Enhancing the Sensitivity of Frequency and Energy Splitting Detection by Using Exceptional Points: Application to Microcavity Sensors for Single-Particle Detection, Phys. Rev. Lett. **112**, 203901 (2014).
[20] H. Hodaei, A. U. Hassan, S. Wittek, H. Garcia-Gracia, R. El-Ganainy, D. N. Christodoulides, and M. Khajavikhan, Enhanced sensitivity at higher-order exceptional points, Nature (London) **548**, 187 (2017).
[21] W. Chen, S. K. Ozdemir, G. Zhao, J. Wiersig, and L. Yang, Exceptional points enhance sensing in an optical microcavity, Nature (London) **548**, 192 (2017).
[22] H. Zhao, Z. Chen, R. Zhao, and L. Feng, Exceptional point engineered glass slide for microscopic thermal mapping, Nat. Commun. **9**, 1764 (2018).
[23] P.-Y. Chen, M. Sakhdari, M. Hajizadegan, Q. Cui, M. M.-C. Cheng, R. El-Ganainy, and A. Alù, Generalized parity-time symmetry condition for enhanced sensor telemetry, National electronics review **1**, 297 (2018).
[24] Z. Dong, Z. Li, F. Yang, C.-W. Qiu, and J. S. Ho, Sensitive readout of implantable microsensors using a wireless system locked to an exceptional point, National electronics review **2**, 335 (2019).
[25] C. Zeng, Y. Sun, G. Li, Y. Li, H. Jiang, Y. Yang, and H. Chen, Enhanced sensitivity at high-order exceptional points in a passive wireless sensing system, Opt. Express **27**, 27562 (2019).
[26] Y.-H. Lai, Y.-K. Lu, M.-G. Suh, Z. Yuan, and K. Vahala, Observation of the exceptional-point-enhanced Sagnac effect, Nature (London) **576**, 65 (2019).
[27] M. P. Hokmabadi, A. Schumer, D. N. Christodoulides, and M. Khajavikhan, Non-Hermitian ring laser gyroscopes with enhanced Sagnac sensitivity, Nature (London) **576**, 70 (2019).
[28] C. M. Bender, D. C. Brody, H. F. Jones, and B. K. Meister, Faster than Hermitian Quantum Mechanics, Phys. Rev. Lett. **98**, 040403 (2007).
[29] C. M. Bender, D. C. Brody, J. Caldeira, U. Günther, B. K. Meister, and B. F. Samsonov, $\mathcal{PT}$-symmetric quantum state discrimination, Phil. Trans. R. Soc. A **371**, 20120160 (2013).
[30] Y. C. Lee, M. H. Hsieh, S. T. Flammia, and R. K. Lee, Local $\mathcal{PT}$ symmetry Violates the No Signaling Priciple, Phys. Rev. Lett. **112**, 130404 (2014).
[31] J.-S. Tang *et al.*, Experimental investigation of the nosignalling principle in parity-time symmetric theory using an open quantum system, Nat. Photonics **10**, 642 (2016).
[32] L. Xiao *et al.*, Observation of topological edge states in parity-time-symmetric quantum walks, Nat. Phys. **13**, 1117 (2017).
[33] U. Günther and B. F. Samsonov, Naimark-Dilated $\mathcal{PT}$-Symmetric Brachistochrone, Phys. Rev. Lett. **101**, 230404 (2008).
[34] K. Kawabata, Y. Ashida, and M. Ueda, Information Retrieval and Criticality in Parity-Time-Symmetric Systems, Phys. Rev. Lett. **119**, 190401 (2017).
[35] Y. Wu, W. Liu, J. Geng, X. Song, X. Ye, C.-K. Duan, X. Rong, and J. Du, Observation of parity-time symmetry breaking in a single-spin system, Science **364**, 878 (2019).
[36] M. Huang, R.-K. Lee, L. Zhang, S.-M. Fei, and J. Wu, Simulating Broken $\mathcal{PT}$-Symmetric Hamiltonian Systems by Weak Measurement, Phys. Rev. Lett. **123**, 080404 (2019).
[37] J. S. Lundeen, B. Sutherland, A. Patel, C. Stewart, and C. Bamber, Direct measurement of the quantum wavefunction, Nature (London) **474**, 188 (2011).
[38] W. W. Pan *et al.*, Direct Measurement of a Nonlocal Entangled Quantum State, Phys. Rev. Lett. **123**, 150402 (2019).
[39] G. S. Thekkadath, L. Giner, Y. Chalich, M. J. Horton, J. Banker, and J. S. Lundeen, Direct Measurement of the Density Matrix of a Quantum System, Phys. Rev. Lett. **117**, 120401 (2016).
[40] Since s and r are parameters in Hamiltonian, they should have the unit of energy. θ is a phase parameter, so it is non-unit. ϵ is the parameter in pertubation of Hamiltonian, concretely, it is always added to s, therefore, it has the same unit as s, i.e., energy unit. Units of other variables, such as $\langle\tilde{H}\rangle_w$, $E_\pm$, ΔE_{EP} and ΔE_{DP}, can be deduced from units of these parameters. Specially, the normalized variable $\Delta E = \Delta E_{EP}/|\Delta E_{DP}|$ is non-unit. Here since we are discussing a general model, and no specific energy or other units are referred to, for simplicity, all the units are omitted, which will not affect the results and readability of this letter.
[41] See Supplemental Material at http://link.aps.org/supplemental/10.1103/PhysRevLett.125.240506 for detailed results, which include (i) details on logic diagram and experimental setup; (ii) relation between the expectation value and the weak value; (iii) weak measurement of the dilated Hamiltonian; (iv) construction of a unitary evolution; (v) deviation between the experimental and theoretical system; (vi) the eigenenergies of the $\mathcal{PT}$-symmetric Hamiltonian; (vii) detailed information about the quantum $\mathcal{PT}$-enhanced sensor; (viii) discussions on the influence of noises to the sensitivity enhancement; (ix) sensitivity enhancement with varying θ; and (x) additional discussions

on the usefulness of the quantum $\mathcal{PT}$-enhanced sensor and its possible applications. Supplemental Material includes Refs. [19,35,36,42–49].

[42] C. L. Degen, F. Reinhard, and P. Cappellaro, Quantum sensing, Rev. Mod. Phys. **89**, 035002 (2017).

[43] R. Demkowicz-Dobrzanski and L. Maccone, Using Entanglement Against Noise in Quantum Metrology, Phys. Rev. Lett. **113**, 250801 (2014).

[44] Z. Huang, C. Macchiavello, and L. Maccone, Usefulness of entanglement-assisted quantum metrology, Phys. Rev. A **94**, 012101 (2016).

[45] H.-K. Lau and A. A. Clerk, Fundamental limits and non-reciprocal approaches in non-Hermitian quantum sensing, Nat. Commun. **9**, 4320 (2018).

[46] W. Langbein, No exceptional precision of exceptional-point sensors, Phys. Rev. A **98**, 023805 (2018).

[47] C. Chen, L. Jin, and R.-B. Liu, Sensitivity of parameter estimation near the exceptional point of a non-Hermitian system, New J. Phys. **21**, 083002 (2019).

[48] M. Zhang, W. Sweeney, C. W. Hsu, L. Yang, A. D. Stone, and L. Jiang, Quantum Noise Theory of Exceptional Point Amplifying Sensors, Phys. Rev. Lett. **123**, 180501 (2019).

[49] F.-F. Yan, J.-F. Wang, Q. Li, Z.-D. Cheng, J.-M. Cui, W.-Z. Liu, J.-S. Xu, C.-F. Li, and G.-C. Guo, Coherent control of defect spins in silicon carbide above 550 K, Phys. Rev. Applied **10**, 044042 (2018).

[50] The parameter s in the Hamiltonian corresponds to the angle setting of wave plates in these two four-port interferometers, therefore, the detected quantity of this experiment (i.e., ϵ) corresponds to a slight change of this angle setting. Details can be found in the Supplemental Material [41].

[51] F. Shi *et al.*, Single-protein spin resonance spectroscopy under ambient conditions, Science **347**, 1135 (2015).

[52] We detect the real and imaginary parts of ΔE separately but not the absolute value $|\Delta E|$ in this experiment, because there always is a part being zero and the other part contains the full information of enhancement. By observing which part (real or imaginary) is vanished, we can determine the additional information that what sign of the perturbation ϵ is. This is another advantage over the conventional sensor.